

A Decentralized Fusion Scheme for 5G Multi-BS Positioning

Sharief Saleh^{ID}, *Graduate Student Member, IEEE*, Qamar Bader^{ID}, *Graduate Student Member, IEEE*
 Mohamed Elhabiby^{ID}, *Member, IEEE* Aboelmagd Noureldin^{ID}, *Senior Member, IEEE*

Abstract—Fifth generation (5G) networks are expected to provide high precision positioning estimation utilizing mmWave signals in urban and downtown areas. In such areas, 5G base stations (BSs) will be densely deployed, allowing for line-of-sight (LOS) communications between the user equipment (UE) and multiple BSs at the same time. Having access to a plethora of measurement sources grants the need for optimal integration between the BSs to have an accurate and precise positioning solution. Traditionally, 5G multi-BS fusion is conducted via an extended Kalman filter (EKF), that directly utilizes range and angle measurements in a centralized integration scheme. Such measurements have a non-linear relationship with the positioning states of the filter, giving rise to linearization errors. Counter to the common belief, an unscented Kalman filter (UKF) will fail to totally eradicate such linearization errors. In this paper, we argue that a de-centralized integration between 5G BSs would fully avoid linearization errors and would enhance the positioning performance significantly. This is done by fusing position measurements as opposed to directly fusing range and angle measurements, which inherently leads to a linear measurement model by design. The proposed de-centralized KF method was evaluated in a quasi-real simulation setup provided by Siradel using a real trajectory in Downtown Toronto. The experiments compared the performance of de-centralized KF integration to that of centralized EKF and UKF integration schemes. It was shown that the proposed method was able to outperform both UKF and EKF implementations in multiple scenarios as it decreased the RMS and maximum 2D positioning errors significantly, achieving decimeter-level of accuracy for 90.3% of the time.

Index Terms—5G; angle of departure (AoD); autonomous vehicles (AVs); decentralized sensor fusion; Kalman filter (KF); mm-Wave; positioning; round trip time (RTT).

I. INTRODUCTION

PRECISE positioning and navigation solutions are becoming of considerable importance in recent years due to the growing research in highly-intelligent internet of things (IoT) applications, context-aware services, and location-based services (LBS). Additionally, precise position information is necessary for safety-critical applications including self-driving cars; which require higher levels of autonomy. Such systems compel centimeter-level of absolute and relative positioning

Sharief Saleh, Qamar Bader, and Aboelmagd Noureldin are with the Department of Electrical and Computer Engineering, Queen's University, Kingston, ON K7L 3N6, Canada, and also with the Navigation and Instrumentation (NavINST) Lab, Department of Electrical and Computer Engineering, Royal Military Collage of Canada, Kingston, ON K7K 7B4, Canada (e-mail: sharief.saleh@queensu.ca; qamar.bader@queensu.ca; nourelda@queensu.ca).

Mohamed Elhabiby is with Micro Engineering Tech. Inc., and also with the Public Works Department, Ain Shams University, Cairo 11566, Egypt (e-mail: mmelhabibi@ucalgary.ca).

accuracy, low latency, and high reliability [1]. Wireless-based positioning has been utilized for decades to provide positioning solutions for applications where high accuracy is subordinate. Such technologies utilize time-, angle-, and power-based measurements to find the user equipment's (UE) position by means of trilateration, triangulation, and hybrid positioning techniques [2]. Trilateration employs ranges acquired by three or more base stations (BSs) to obtain the position of the UE. Triangulation, on the other hand, exploits multiple relative angle measurements to estimate the position of the UE. Lastly, hybrid positioning approaches utilize both range and angle measurements to get the location of the user, which can be achieved through a single BS. Global navigation satellite systems (GNSS) for instance, can provide a few-meter level of accuracy in standalone operation, and down to cm-level of accuracy when aided by real-time kinematic (RTK) technology [3]. However, GNSS-based positioning solutions deteriorate in urban canyon environments due to multi-path and signal blockage. On the other hand, WiFi and ultra-wide band (UWB) are capable of attaining sub-meter level of accuracy, yet, both technologies suffer from short-range operation ranging between 50m to 200m [4] [5], rendering them advantageous only in indoor environments. On the contrary, 5G new radio (NR) has a large bandwidth of up to 400 MHz, yielding accurate time-based measurements estimation, such as time of arrival (ToA), round trip time (RTT), and time difference of arrival (TDoA), as well as high multi-path (MP) resolvability in the time domain. Additionally, as 5G frequency range 2 (FR2) operates on high-frequency mmWave signals spanning from 28GHz to 52GHz, allowing for the emergence of massive MIMO. Thus, 5G receivers will comprise a large number of antennas enabling accurate angle-based measurements such as angle of arrival (AoA) and angle of departure (AoD), as well as high MP resolvability in the angle domain. Moreover, 5G gNodeBs (gNbs) are to be deployed densely by means of small-cell densification, with 200 to 500 meters inter-cell distance. This will increase the chance of line-of-sight (LoS) communications with the user [6].

In order to optimize the estimation of the UE's position considering the noisy range and angle measurements, optimal state estimators are needed. The most commonly used filters are the Kalman filter (KF) [7], the extended Kalman filter (EKF) [8], the unscented Kalman filter (UKF) [9], and the particle filter (PF) [10]. While KF assumes the linearity of both the state transition and the observation models, the remaining stated filters do not oblige the same requirement. Additionally, KF, EKF, and UKF assume normally distributed process noise

and measurement noise to function optimally. Despite the fact that PF does not enforce any restrictions or assumptions of the process/measurement model, it is typically avoided due to its high computation complexity. All of the aforementioned filters can be utilized in centralized or decentralized state estimation schemes, also known as tightly coupled (TC) and loosely coupled (LC) integration schemes respectively. TC and LC integration schemes are well-known in the GNSS/INS community. Centralized/TC schemes integrate all technologies/BSs on the measurement level within a single-stage filter. Decentralized/LC schemes, on the other hand, involve multi-stage positioning where each technology/BS computes its own estimate of the position, and then integration on the position level takes place in a cascaded manner.

The contributions of this paper are as follows:

- 1) We present an extensive analysis of the drawbacks of centralized/TC integration schemes.
- 2) A novel decentralized/LC multi-BS 5G positioning approach is proposed, which will avoid the disadvantages of centralized integration schemes.
- 3) For validation, we assess three Bayesian estimators, namely, LC-KF, TC-EKF, and TC-UKF in a quasi-real testing environment.

The remainder of the paper is organized as follows: Section II presents previous works related to 5G positioning using optimal estimators. Section III establishes the system model and the basics of 5G positioning. Section IV exhibits the various implementations of Kalman filters and Section V thoroughly analyzes centralized fusion schemes and proposes 5G decentralized integration as a strong contender. Section VI provides details on the experimental setup and presents the results along with discussions. Finally, Section VII concludes the paper.

II. LITERATURE REVIEW

Various works have investigated 5G positioning using different estimation techniques that adopt a centralized integration scheme. Authors in [11] used EKF to estimate the UE's position employing AoD and ToA measurements, giving rise to high linearization errors due to the use of highly non-linear observation models, achieving sub-meter accuracy for 75% of the time. In [12], [13] an accuracy of sub-meter level was accomplished for 90% of the time through utilizing TDoA trilateration. However, this was achieved assuming that the UE is connected to three BSs simultaneously at all times, which is an impractical assumption. Authors in [14] proposed a hybrid positioning scheme based on TDoA, and AoA using an EKF, achieving sub-3-meter level of accuracy for 95% of the time. Nevertheless, it still endures the same limitations as observed in previous works. In [14], authors have utilized TDoA and AoA measurements and achieved sub-3 meters of accuracy 95% of the time. The work in [15] has mitigated some of these limitations by endorsing a non-linear state transition model (NLSTM) as an alternative to the constant velocity model. This model makes use of the forward velocity of the vehicle and its heading angle to estimates the vehicle's position. The proposed NLSTM surpassed former works, attaining sub-2.3 meters of

accuracy for 95% of the time. Limited work was done on the use of Unscented Kalman Filter (UKF) for 5G standalone positioning. In [16] a UKF-based estimator was employed to estimate AoA and ToA, and 3D device positioning, accomplishing sub-meter level of accuracy. Nevertheless, they have assumed BSs are deployed every 50m, which does not follow the standard for small cells deployed in urban areas as seen in [17]. All of the aforementioned works utilize tightly coupled schemes to integrate between the BSs' raw time and angle measurements. This will prove detrimental to the accuracy of the 5G positioning solution.

III. SYSTEM MODEL

5G NR has enhanced the LTE's downlink (DL) positioning reference signal (PRS) and uplink (UL) sounding reference signal (SRS) to allow for more precise positioning measurements. With the aid of these signals, ToA, RTT, and TDoA are computed through correlation with the configured reference signal. UL-AoA can be estimated through the Multiple Signal Classification (MUSIC) algorithm or through the estimation of signal parameters using rotational invariance techniques (ESPRIT) by utilizing UL-SRS. Moreover, AoD is inherently computed within the beamforming training sequence by comparing the received power of multiple PRS signals. In this paper, the authors consider positioning at the UE side, and thus, DL-PRS signals are utilized to compute DL-AoD and RTT measurables. Such measurables are then used to compute the relative distance between the UE and the BS (r), as well as the azimuth angle (θ) as seen in (1) and (2).

$$r = \sqrt{\Delta x^2 + \Delta y^2 + \Delta z^2} \quad (1)$$

$$\theta = \arctan \left(\frac{\Delta y}{\Delta x} \right) \quad (2)$$

Where $(\Delta x, \Delta y, \Delta z)$ denote the difference between the UE's position (x, y, z) and the BS position (x_{BS}, y_{BS}, z_{BS}) . Next, the range and angle measurements offered by each connected BS can either be fused in a centralized or a decentralized fashion. In centralized fusion, all ranges and angles are fused in a single filter to compute the UE's position as seen in Fig. 1. On the other hand, in decentralized fusion, the UE first computes multiple position estimates by using an open-loop geometry-based calculation using the individual BSs' measurables. Next, an optimal estimator fuses these position estimates into a single position estimate as seen in Fig. 2.

In order to compute the 3D position of a vehicle for decentralized fusion using a single BS, the range, the azimuth angle, and the elevation angles are required as seen below:

$$\begin{aligned} x &= r \cdot \sin(\theta) \cos(\phi) + x_{BS} \\ y &= r \cdot \cos(\theta) \cos(\phi) + y_{BS} \\ z &= r \cdot \sin(\phi) + z_{BS} \end{aligned} \quad (3)$$

Where ϕ is the elevation angle. In order to measure the elevation angle along with the azimuth angle of departure, a 2D uniform rectangular array (URA) of antennas would be

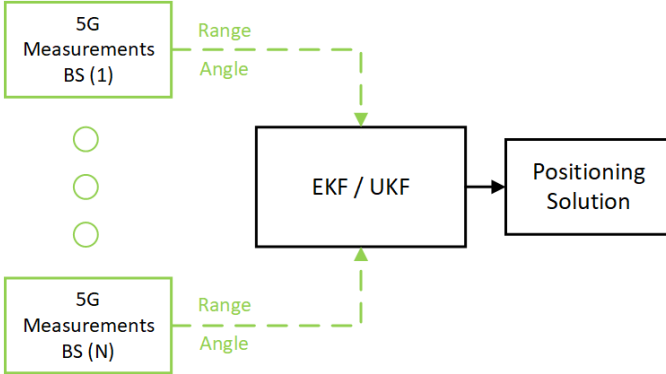


Fig. 1. Block diagram of centralized 5G multi-BS integration.

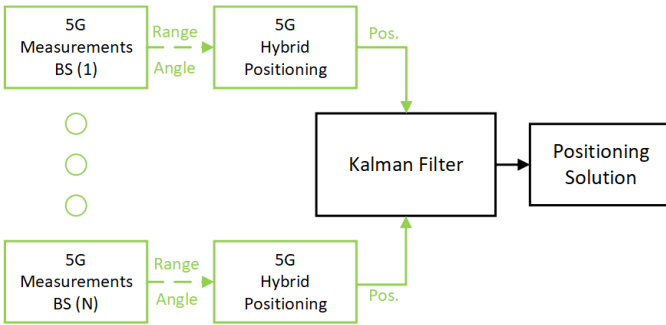


Fig. 2. Block diagram of decentralized 5G multi-BS integration.

required. Alternatively, if the height of the vehicle is known to be constant, then the requirement for knowledge of elevation angle can be alleviated. Thus, requiring only a 1D uniform linear array (ULA). Such assumption usually holds true for land vehicles, as changes in the Z-axis are generally minute. The position of the vehicle can thus be computed as follows:

$$\begin{aligned} x &= r_{2D} \cdot \sin(\theta) + x_{BS} \\ y &= r_{2D} \cdot \cos(\theta) + y_{BS} \\ r_{2D} &= \sqrt{r^2 - \Delta z^2} \end{aligned} \quad (4)$$

Where r_{2D} is the 2D range between the BS and the UE, and Δz is the known height difference between the BS and the UE.

Finally, in order to explore the true potential of 5G-NR's small-cell densification, the setting of autonomous driving was set to be in downtown areas where urban canyons and high-rise buildings surround the vehicle. Such a setting entails that a UE might be connected to a maximum of three BSs at a time. It also imposes the possibility of having access to a single BS at times and total loss of LOS connection to all BSs in rare cases. Thus, an NLOS detection algorithm based on range comparison between RTT and RSS measurements, proposed in [18], will be utilized to exclude NLOS BSs.

IV. KALMAN FILTER REALIZATIONS

The Kalman filter is an optimal iterative estimator for linear systems with Gaussian noise, illustrated in Alg. 1. With these two assumptions, the KF is able to propagate, transform, and

manipulate the states' probability density function (PDF) by only tracking their mean and covariance expressed by \mathbf{X} and \mathbf{P} respectively. The KF consists of two consecutive stages of state prediction and correction. In the state prediction stage, the KF propagates the a posteriori state estimate and covariance matrix, \mathbf{X}_{k-1}^+ and \mathbf{P}_{k-1}^+ respectively, from the previous epoch, to the current epoch k via the transition matrix \mathbf{F} . The outputs of such transformation are the a priori state estimate \mathbf{X}_k^- and the covariance matrix \mathbf{P}_k^- . Since such a process of state transformation is not perfect, the process covariance matrix \mathbf{Q} is also added to the a priori covariance matrix with the aid of the noise coupling matrix \mathbf{G} . The state correction stage utilizes the measurement vector \mathbf{Z}_k along with the Kalman gain \mathbf{K}_k to update the a priori state and covariance estimate into a posteriori estimates \mathbf{X}_k^+ and \mathbf{P}_k^+ . The Kalman gain \mathbf{K}_k is computed with the aid of \mathbf{P}_k^- and the measurement covariance matrix \mathbf{R} . Moreover, the measurement observation matrix \mathbf{H}_k is used to transform \mathbf{P}_k^- and \mathbf{X}_k^- from the state domain to the measurement domain and vice versa.

Algorithm 1: Kalman Filter

```

initialization:  $\mathbf{X}_0^+, \mathbf{P}_0^+, \mathbf{Q}, \mathbf{R}, k = 0$ 
while positioning do
     $k = k + 1$ 
     $\mathbf{X}_k^- = \mathbf{F}\mathbf{X}_{k-1}^+$ 
     $\mathbf{P}_k^- = \mathbf{F}\mathbf{P}_{k-1}^+\mathbf{F}^T + \mathbf{G}\mathbf{Q}\mathbf{G}^T$ 
     $\mathbf{K}_k = \mathbf{P}_k^-\mathbf{H}_k^T(\mathbf{H}_k\mathbf{P}_k^-\mathbf{H}_k^T + \mathbf{R})^{-1}$ 
     $\mathbf{X}_k^+ = \mathbf{X}_k^- + \mathbf{K}_k(\mathbf{Z}_k - \mathbf{H}_k\mathbf{X}_k^-)$ 
     $\mathbf{P}_k^+ = \mathbf{P}_k^- + \mathbf{K}_k\mathbf{H}_k\mathbf{P}_k^-$ 
end
  
```

It is worth noting that the main difference between KF and EKF is that EKF deals with non-linear transition models and non-linear state-measurement models. In case of encountering non-linearity in the transition model, $f(\mathbf{X}_{k-1}^+)$ is used to translate the state instead of $\mathbf{F}\mathbf{X}_{k-1}^+$, and \mathbf{F} is computed by finding the Jacobian of $f(\mathbf{X})$. Likewise, in case of encountering non-linearity between the states and the measurements, then $h(\mathbf{X}_k^-)$ is used instead of $\mathbf{H}_k\mathbf{X}_k^-$ to transform the states to measurements, and \mathbf{H}_k is computed by finding the Jacobian of $h(\mathbf{X})$.

The use of UKF resolves the non-linear approximation drawbacks of the EKF by transforming the state's PDFs through non-linear functions. The UKF conducts PDF transformation by generating $2N + 1$ sigma points χ_k , where N is the number of connected BSs. Then, the UKF propagates the individual χ_k points through the non-linear function, and finally computes the mean and covariance of the propagated points to find \mathbf{X} and \mathbf{P} respectively. The UKF algorithm is illustrated in Alg. 2.

V. 5G MULTI-BS SENSOR FUSION

A. States and State Transition Process

The navigation states considered in all methodologies presented in this paper comprise of the estimated 2D position

Algorithm 2: Unscented Kalman Filter

initialization: $\mathbf{X}_0^+, \mathbf{P}_0^+, \mathbf{Q}, \mathbf{R}, W_m^i, \lambda, k = 0$
while positioning **do**

$$\begin{aligned}
k &= k + 1 \\
\mathbf{x}_k^{-(i)} &= [\hat{\mathbf{X}}_{k-1}^+ \pm \sqrt{\lambda + N} [\sqrt{\mathbf{P}_{k-1}^+}]] \\
\mathbf{X}_k^{(i)} &= f(\mathbf{x}_k^{-(i)}) ; i = 0, 1, \dots, 2N \\
\hat{\mathbf{X}}_k^- &= \sum_{i=0}^{2N} W_m^i \mathbf{X}_k^{(i)} \\
\mathbf{P}_k^- &= \sum_{i=0}^{2N} W_m^i (\mathbf{X}_k^{(i)} - \hat{\mathbf{X}}_k^-) (\mathbf{X}_k^{(i)} - \hat{\mathbf{X}}_k^-)^T + \mathbf{Q} \\
\mathbf{Z}_k^{(i)} &= h(\mathbf{X}_k^{(i)}) \\
\hat{\mathbf{Z}}_k &= \sum_{i=0}^{2N} W_m^i \mathbf{Z}_k^{(i)} \\
\mathbf{P}_z &= \sum_{i=0}^{2N} W_m^i (\mathbf{Z}_k^{(i)} - \hat{\mathbf{Z}}_k^-) (\mathbf{Z}_k^{(i)} - \hat{\mathbf{Z}}_k^-)^T + \mathbf{R} \\
\mathbf{P}_{xz} &= \sum_{i=0}^{2N} W_m^i (\mathbf{X}_k^{(i)} - \hat{\mathbf{X}}_k^-) (\mathbf{Z}_k^{(i)} - \hat{\mathbf{Z}}_k^-)^T \\
\mathbf{K}_k &= \mathbf{P}_{xz} \mathbf{P}_z^{-1} \\
\hat{\mathbf{X}}_k^+ &= \mathbf{X}_k^- + \mathbf{K}_k (\mathbf{Z}_k + \hat{\mathbf{Z}}_k) \\
\mathbf{P}_k^+ &= \mathbf{P}_k^- + \mathbf{K}_k \mathbf{P}_z^- \mathbf{K}_k^T
\end{aligned}$$

end

and velocity of the UE, i.e. $\mathbf{X} = [x, y, v_x, v_y]^T$. Likewise, the state transition process for all KF implementations in this work considers a constant velocity model, yielding a linear state transition model as seen in (5). Since the state transition model is linear, then $f(\mathbf{X})$ is equivalent to $\mathbf{F}\mathbf{X}$, which is used by UKF to propagate the state's sigma points from epoch $k-1$ to epoch k .

$$\mathbf{F} = \begin{bmatrix} 1 & 0 & \Delta t & 0 \\ 0 & 1 & 0 & \Delta t \\ 0 & 0 & 1 & 0 \\ 0 & 0 & 0 & 1 \end{bmatrix} \quad (5)$$

The process covariance matrix \mathbf{Q} comprises the errors arising due to violating the constant velocity model by either changing the orientation of the vehicle or by accelerating / decelerating. Thus, \mathbf{Q} was set by empirically computing the average variance of the velocity of vehicles driving in a downtown setting. The experimental setup used for such empirical tuning of \mathbf{Q} is detailed in section VI. On the other hand, \mathbf{R} comprises measurement errors. For centralized integration, \mathbf{R} consists of the noise variance of the range and angle measurements. In this work, range measurements had a variance of $1mm$ and angle measurements had a variance of 0.1° . In decentralized integration, however, \mathbf{R} noise of the position estimates of each BS, which was set to be $1cm$ for both x and y measurements.

B. Centralized Integration

In centralized 5G multi-BS sensor fusion, the raw range and angle measurements are directly fused together in the fusion filter as seen in Fig. 1. The measurement vector \mathbf{Z} for both

EKF and UKF centralized implementations will be as follows: $\mathbf{Z} = [r_1, \theta_1, \dots, r_N, \theta_N]^T$. The non-linear measurement model of the system for both EKF and UKF is expressed in (6). Furthermore, the Jacobian matrix $\mathbf{H}_k \in \mathbb{R}^{2N \times 4}$ is computed using Taylor series expansion as seen in (7). It is worth noting that \mathbf{H}_k is only utilized for the centralized EKF implementation. Linearization errors due to the use of non-linear measurement models will be discussed further in the consequent subsections.

$$\mathbf{h}(\mathbf{X}) = \begin{bmatrix} \sqrt{(\Delta x_k[n])^2 + (\Delta y_k[n])^2} \\ \arctan\left(\frac{\Delta y_k[n]}{\Delta x_k[n]}\right) \end{bmatrix} \quad (6)$$

$$\mathbf{H}_k = \begin{bmatrix} \frac{dx_1}{r_1} & \frac{dy_1}{r_1} & 0 & 0 \\ -\frac{dy_1}{r_1^2} & \frac{dx_1}{r_1^2} & 0 & 0 \\ \vdots & \vdots & \vdots & \vdots \\ \frac{dx_N}{r_N} & \frac{dy_N}{r_N} & 0 & 0 \\ -\frac{dy_N}{r_N^2} & \frac{dx_N}{r_N^2} & 0 & 0 \end{bmatrix} \quad (7)$$

C. Proposed Decentralized Integration

Decentralized integration of multiple BSs is viewed by the author as one of the main advantages of 5G-NR. Decentralized integration schemes were not attainable for GNSS-based systems in the past, as individual satellites do not have the ability to estimate the position of the UE using a single range measurement. Thus, GNSS systems were forced to use centralized fusion schemes along with their inevitable linearization errors. On the contrary, individual 5G BSs are capable of providing independent estimates of the position of the UE, enabling decentralized integration of BSs, where the relationship between the states and the measurements is linear. In decentralized 5G multi-BS sensor fusion, the measurement vector \mathbf{Z} will be as follows: $\mathbf{Z} = [x_1, y_1, \dots, x_N, y_N]^T$, hence, the linear relationship between the states and measurements. The \mathbf{H}_k matrix for a decentralized fusion of 5G BSs is presented in (8). It is worth noting that despite its simplistic and elegant design, the 5G positioning literature has failed to propose such a scheme. Thus, in this paper, we propose the use of decentralized integration schemes for 5G multi-BS positioning as it eliminates linearization errors without incurring any downsides in return.

$$\mathbf{H} = \begin{bmatrix} 1 & 0 & 0 & 0 \\ 0 & 1 & 0 & 0 \\ \vdots & \vdots & \vdots & \vdots \\ 1 & 0 & 0 & 0 \\ 0 & 1 & 0 & 0 \end{bmatrix} \quad (8)$$

D. Linearization Errors

Linearization errors are inevitable to occur in centralized integration of 5G BSs using raw measurements such as the range and angle. As already established, the Jacobian matrix \mathbf{H}_k is computed through Taylor series expansion of $h(\mathbf{X})$. Such a linearization process eliminates higher order terms of range and angle measurements, leading to linearization errors.

\mathbf{H}_k is used in multiple places in Kalman filter implementations as seen in Alg. 1. It is therefore important to study the negative effects imposed by each use of a such linearized version of the measurement observation matrix. It is worth pointing out that a common mistake that is usually encountered in the literature while implementing EKF is the use of \mathbf{H}_k instead of $h(\mathbf{X})$ within the innovation sequence, i.e. the use of $\mathbf{Z}_k - \mathbf{H}_k \mathbf{X}$ instead of $\mathbf{Z}_k - h(\mathbf{X})$. Such a mistake will bias the rather unbiased filter, leading to extra unnecessary errors. With that being said, in EKF implementations, the observation matrix is solely used in the computation of the Kalman gain \mathbf{K} , which has two purposes in the correction process. First, it optimally weights the individual measurement errors in the innovation sequence. Second, it transforms the innovation sequence from the measurement domain to the state domain. The observation matrix \mathbf{H}_k has a role to play in both functions. First, \mathbf{H}_k is utilized to find the innovation covariance matrix $(\mathbf{H}_k \mathbf{P}_k^{-} \mathbf{H}_k^T + \mathbf{R})$. The innovation covariance matrix is essential in the weighting process of the EKF. Therefore, linearization errors in \mathbf{H}_k would lead to a filter that is either overconfident or underconfident about the innovation sequence. It is worth noting that the UKF implementation is free of such errors due to the use of sigma points to compute the innovation covariance matrix. This will lead to a more accurate weighting of the measurements in UKF implementations. The second use of the observation matrix is to help with transforming the innovation residual errors from the measurement domain to the state domain. This is done through the use of \mathbf{H}_k^T . Meaning, the non-linear relationship between the states and the measurements is reduced to a linear multiplication between \mathbf{H}_k^T and $\mathbf{Z}_k - h(\mathbf{X})$. Such simplification of the non-linear relationship will induce high positioning errors in centralized EKF implementations. It is worth noting that the UKF centralized implementation would also suffer from such transformation errors, despite the usage of sigma points to compute the Kalman gain. That is due to the fact that UKF still utilizes linear multiplication between \mathbf{K}_k and $\mathbf{Z}_k - h(\mathbf{X})$ to perform the non-linear transformation. Thus, counter to the common belief, the UKF is not totally immune to linearization errors. As a matter of fact, the authors claim that all KF implementations and variations will suffer from linearization errors to some degree due to the inherent fundamental design of Kalman filters.

To further study the discussed linearization errors, multiple theoretical simulations were conducted. The simulations tackle both weighting and transformation errors for both range and angle measurements. In order to simulate weighting errors, a random number generator was utilized to generate a cloud of normally distributed UE positions with a set mean and variance. The point cloud was then passed once through the non-linear measurement model $h(\mathbf{X})$ and through the linearized measurement model $\mathbf{H}\mathbf{X}$. Finally, the resulting transformed PDFs are displayed for comparison. The PDF resulting from the non-linear transformation acts as the ground truth for what the distribution should ideally look like. Of course, the non-linearly transformed distributions are not expected to be Gaussian as opposed to a linearly transformed distribution. Yet, it is still expected that the linearly transformed distribution

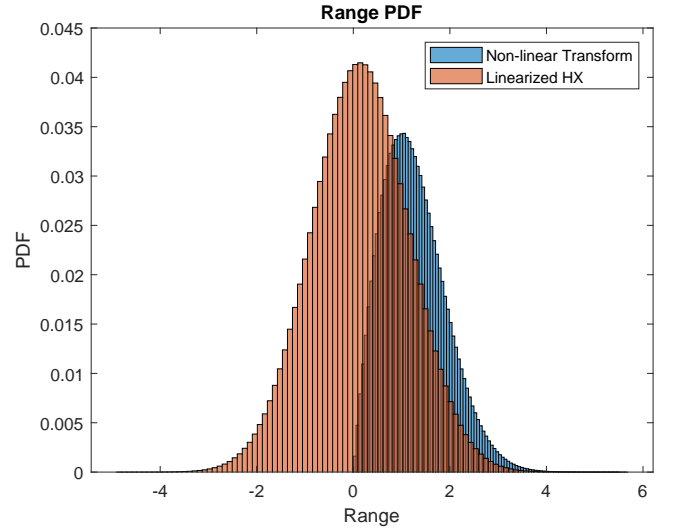


Fig. 3. Transformation of position PDF to range PDF at close BS-UE range ($\Delta x = \Delta y = 0.1m$).

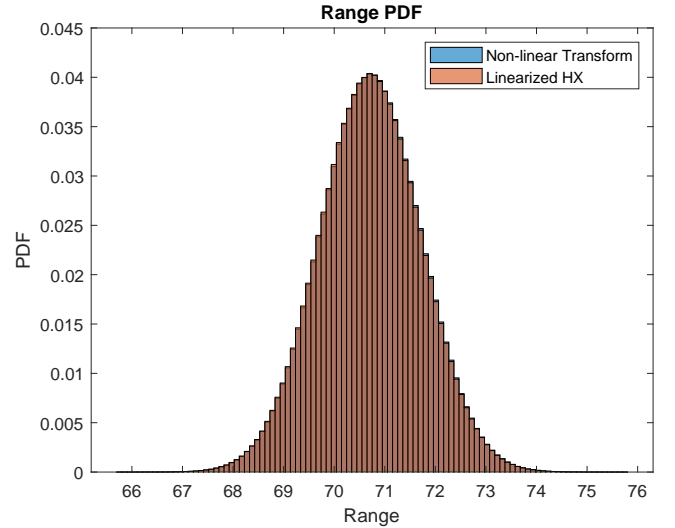


Fig. 4. Transformation of position PDF to range PDF at far BS-UE range ($\Delta x = \Delta y = 50m$).

would be as close as possible to the non-linearly transformed distribution to have a fair weighting of measurements. Figs. 3 and 4 show the simulation for range measurement's PDF transformation at close range and far range respectively. It can be seen that at close ranges, the linearly transformed PDF does not mimic the non-linearly transformed PDF, which was expected according to [19]. More importantly, it can be seen that the linearly transformed PDF possess has higher variance compared to the real variance of non-linear transformation, meaning that the filter will underestimate the correction update. On the other hand, it can be seen that at far ranges, both PDFs are almost identical, resulting in proper weighting of the measurements.

Figs. 5 and 6 present the simulation for angle measurement's

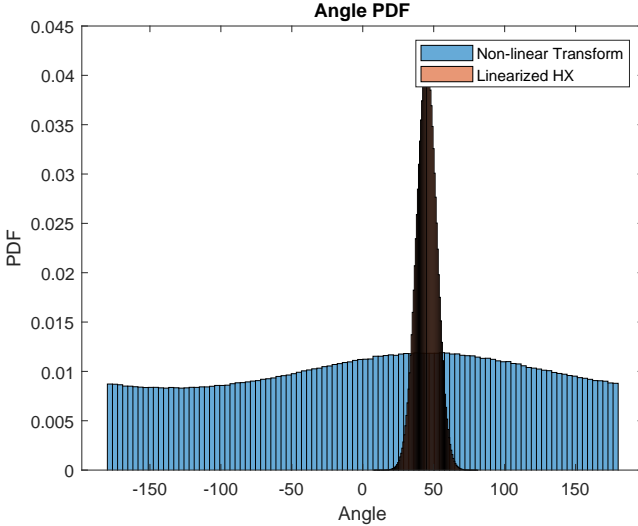


Fig. 5. Transformation of position PDF to angle PDF at close BS-UE range ($\Delta x = \Delta y = 0.1m$).

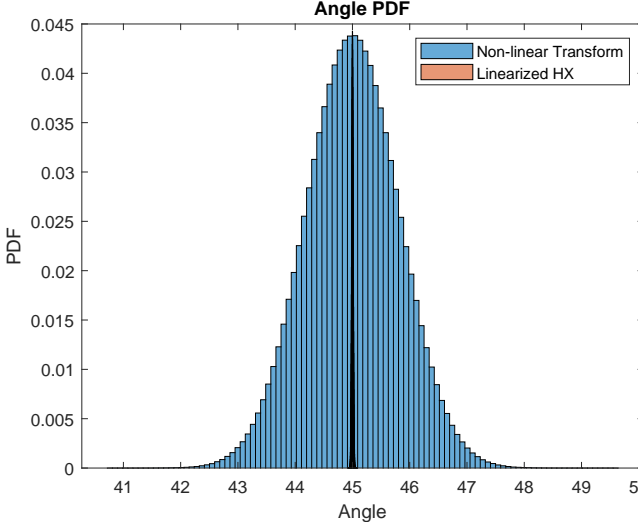


Fig. 6. Transformation of position PDF to angle PDF at far BS-UE range ($\Delta x = \Delta y = 50m$).

PDF transformation at close range and far range respectively. It can be seen that the linearly transformed PDF is heavily overconfident in both scenarios compared to their non-linearly transformed counterparts. Such overconfidence in measurements is dangerous in real-life navigation especially if the update is expected to be biased as well due to the transformation errors.

In order to simulate transformation errors, a mesh of UE positions was created and utilized to compute the range and angle through the non-linear measurement model $h(X)$ and through the linearized measurement model HX . The difference between the two transformations is then presented, which is directly indicative of the linearization error arising from the Taylor series approximation. Figs. 7 and 8 show the

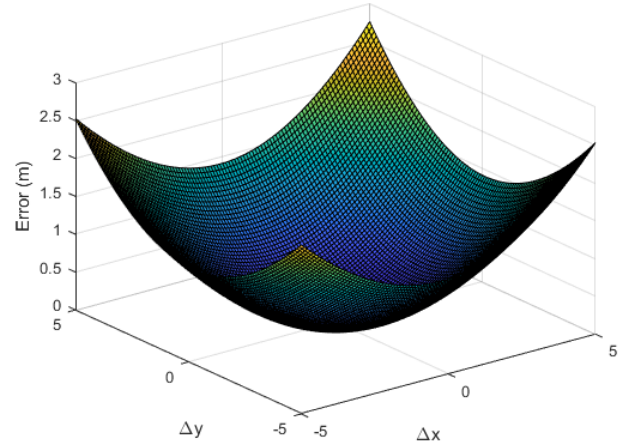


Fig. 7. Range linearization error at close BS-UE range ($\Delta x = \Delta y = 1m$).

linearization errors of range measurements at close and far BS-UE ranges. It is clear that the linearization errors due to linearized transformation do increase in magnitude the closer the UE drives near the BS. Additional analysis on the errors can be found in [19]. Fig. 9 depicts the transformation errors in angle when the linearization was done around $\theta = 45^\circ$. The figure shows a couple of findings. First, linearizing an arc-tan function through the Taylor series approximation would result in a considerable amount of errors that can reach up to 240° . Second, it can be seen that the linearization error was at its lowest when Δx and Δy are equal, which is expected as the linearization was performed around 45° . Third, linearization of the arc-tan function is very sensitive to any errors in the innovation sequence, as linearization errors would dramatically increase when the innovation sequence errors cease to be very close to zero. Hence, it is not advised to linearize such a function if other alternative solutions are available, which is the case with the proposed decentralized integration.

VI. EXPERIMENTAL SETUP AND RESULTS

A. Experimental Setup

In order to verify the superiority of decentralized/LC integration over centralized/TC integration, a quasi-real 5G simulation setup that was provided by Siradel was utilized. Siradel 5G_Channel comprises of LiDAR-based maps of the buildings, vegetation, and water bodies in downtown areas of cities like Toronto, New York, and Paris as seen in Fig. 10. The simulation tool requires the position of the UE and the virtually connected BSs to compute required positioning measurables like RSS, ToA, AoA, and AoD via its ray-tracing capabilities and propagation models. To mimic a true urban navigation scenario, a vehicle was equipped with a high-end positioning solution provided by NovAtel; that includes KVH 1700, a tactical grade IMU, along with NovAtel's tactical grade GNSS receiver, and was driven in Downtown Toronto. The vehicle was driven for 1hr and 13mins, and the trajectory was 9km long as seen in Fig. 11. The trajectory was conducted during

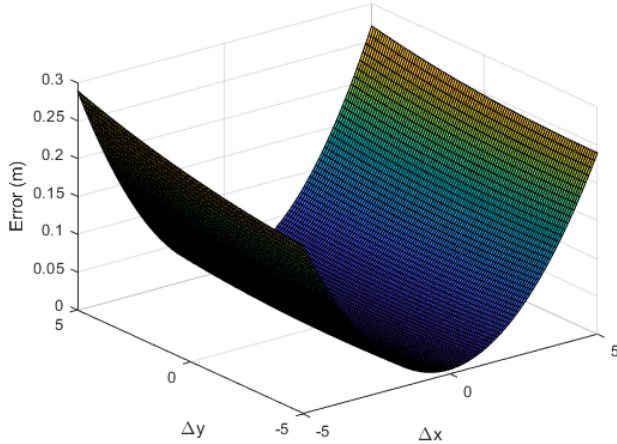


Fig. 8. Range linearization error at far BS-UE range ($\Delta x = 1m$, $\Delta y = 50m$).

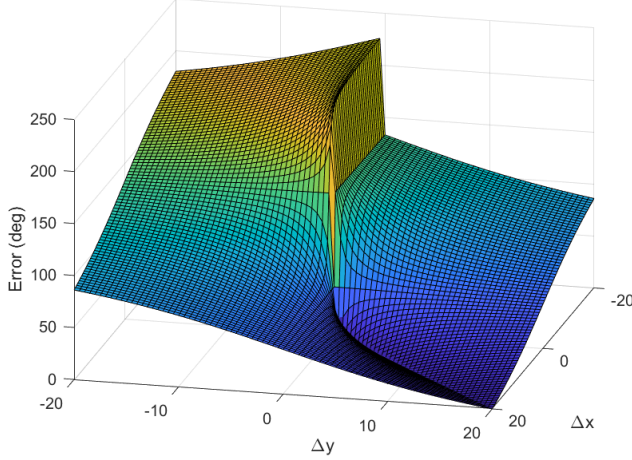


Fig. 9. Angle linearization error at 45° orientation.

rush hour, and thus, many sudden car stopping/acceleration dynamics were encountered. Moreover, the trajectory features many turns and challenging maneuvering dynamics. Next, a code was developed to place BSs along the driven trajectory that are $250m$ apart, as per 3GPP's Release 16 guidelines [20]. Finally, the generated BS positions along with NovAtel's reference solution were imported to Siradel to generate the needed 5G measurables. Siradel was set up to utilize mmWave signals with a carrier frequency around $28GHz$ and a bandwidth of $400MHz$. The BSs were equipped with 8×1 ULAs while the UE was equipped with an omnidirectional antenna.

B. Results and Discussions

In this section, the performance of the centralized schemes using EKF and UKF will be compared to the performance of the proposed decentralized scheme using a KF. The comparison will be done in three scenarios. First, perfect range

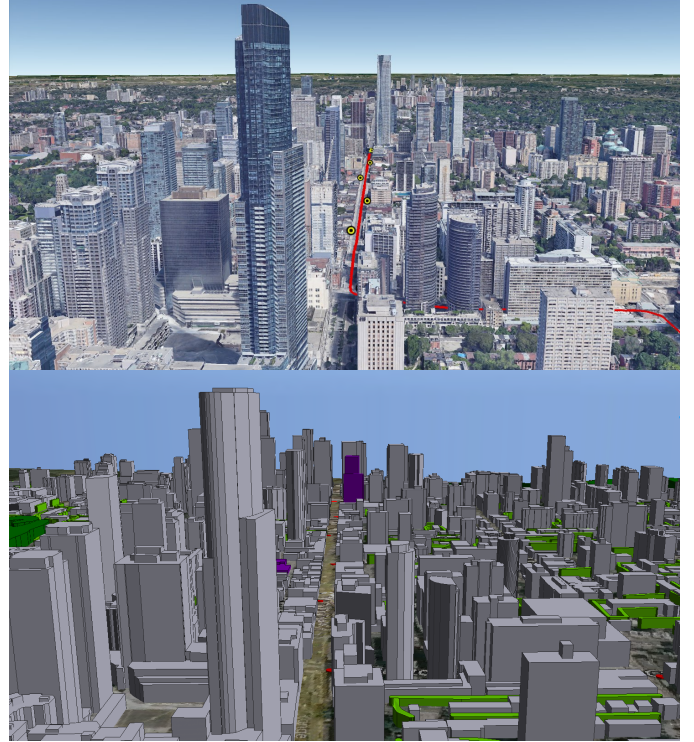


Fig. 10. Downtown Toronto, ON, Google Earth (Top) vs Siradel simulation tool (Bottom).

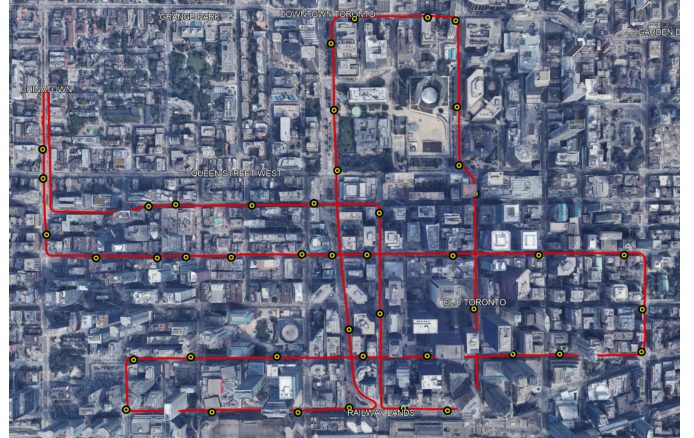


Fig. 11. Downtown Toronto Trajectory (Red), and 5G BSs (Yellow circles).

and angle measurements are supplied to all filters. Positioning errors arising from this test will be solely attributed to linearization errors. The second test scenario will incorporate quasi-real measurements from Siradel's simulations and NLOS communications will be permitted without NLOS detection functionalities. Such a test will show the need for having NLOS detection capabilities as a prerequisite to lane-level positioning. Finally, the third test scenario will include both quasi-real measurements and NLOS detection capabilities discussed in [18]. This will act as an accurate benchmark of the expected performance of the compared filters and integration schemes. For all test scenarios, a trilateration variant solution

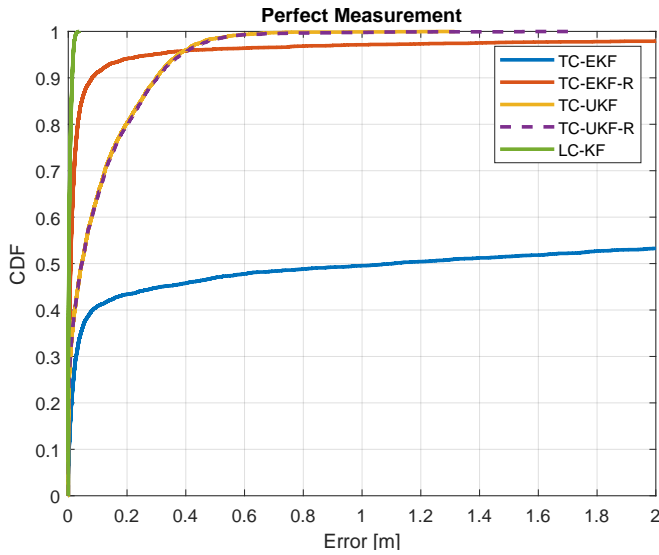


Fig. 12. CDF of the 2D positioning errors while utilizing perfect range and angle measurements.

will also be presented for EKF and UKF solutions; referred to as EKF-R and UKF-R, to gauge the advantages and disadvantages of adding angle measurements to centralized fusion.

Fig. 12 depicts the Cumulative Distribution Function (CDF) of all implemented filters and integration schemes using perfect measurements. It is evident the decentralized KF implementation trumped all other schemes, as it had an almost perfect performance. On the other hand, it can be seen that the EKF hybrid implementation had the lowest performance, even compared to its trilateration counterpart. This proves that linearizing angle-based measurements hinder the performance of the filter as it adds more errors than extra information. Additionally, both UKF implementations had almost similar performance, meaning that adding angle measurements did not add extra value in centralized fusion schemes. Moreover, it is apparent that the UKF had more errors at the decimeter level compared to its EKF counterpart, yet, it was able to suppress errors above 0.5m. To have a deeper insight into how linearization errors affect measurements, two close-up test samples are shown in Figs. 13 and 14, where the UE drives close to BSs. It can be seen that both decentralized KF and centralized UKF did not sustain much error while passing by nearby BSs. On the contrary, the centralized EKF implementation has sustained considerable positioning errors due to linearization errors.

Fig. 15 illustrates the CDF of all implemented filters and integration schemes using real range and angle measurements from Siradel without NLOS detection capabilities. Patently, the proposed decentralized KF implementation has outperformed all other schemes by a remarkable margin. Yet, such performance is not enough to achieve lane-level accuracy, as it was not able to suppress high levels of errors. Meanwhile, all other implementations failed to provide presentable estimations, as they sustained sub-2m level of accuracy less than 26% of the

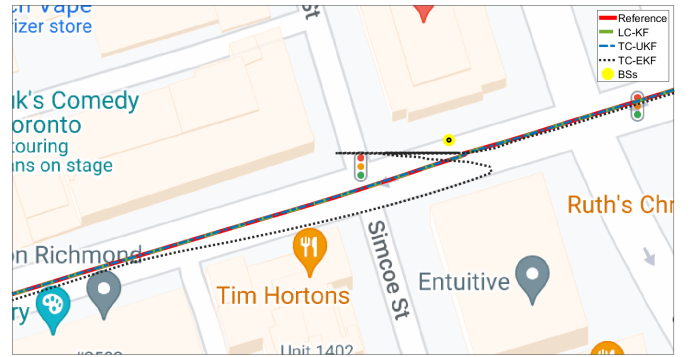


Fig. 13. Close-up performance of filters while driving close to a BS using perfect measurement

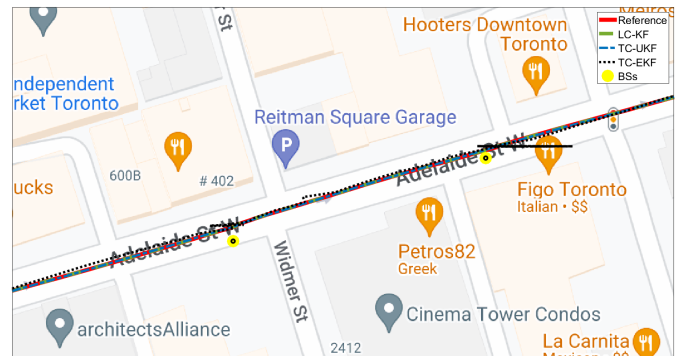


Fig. 14. Close-up performance of filters while driving close to a BS using perfect measurements.

time. This is expected, as linearization errors have a higher impact when the innovation sequence's residual error is high in value, which is the case for NLOS measurements. This finding shows the importance of the development of NLOS detection algorithms, which are not given enough attention in the community. Also, it proves the superiority of the proposed decentralized approach in case the NLOS detector failed to capture an NLOS communication link.

Fig. 16 shows the CDF of the positioning error for all aforementioned schemes while using real Siradel range and angle measurements along with NLOS detection capabilities found in [18]. Evidently, the proposed decentralized KF implementation was able to outperform other implementations in both decimeter level accuracy and in meter level accuracy statistics. The proposed method was able to navigate with a sub-meter level of accuracy for around 91% of the time. Both UKF implementations were able to maintain a sub-1m level of accuracy for around 82% of the time. It is also noticeable that the trilateration-based UKF was slightly better than its hybrid counterpart due to the avoidance of extra linearization errors imposed by the angle measurements. Finally, it is conspicuous beyond doubt that both EKF implementations are unsuitable for lane level positioning, albeit the trilateration version had remarkably better performance for the aforementioned reasons.

Figs. 17-19 show close-up samples of the positioning solu-

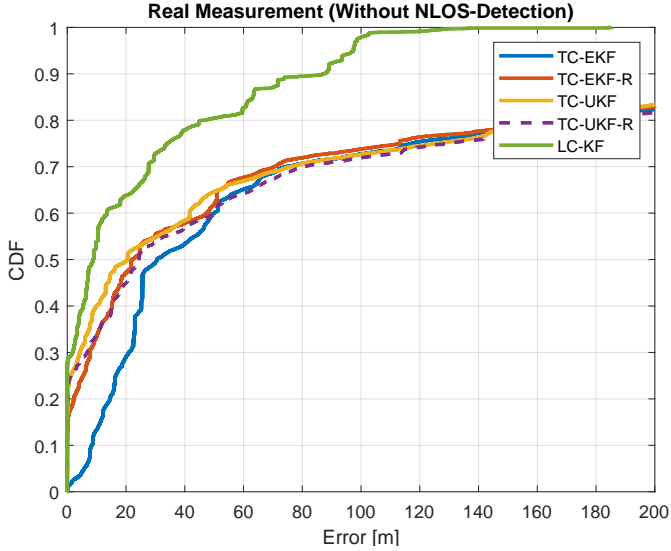


Fig. 15. CDF of the 2D positioning errors while utilizing quasi-real Siradel range and angle measurements without NLoS detection.

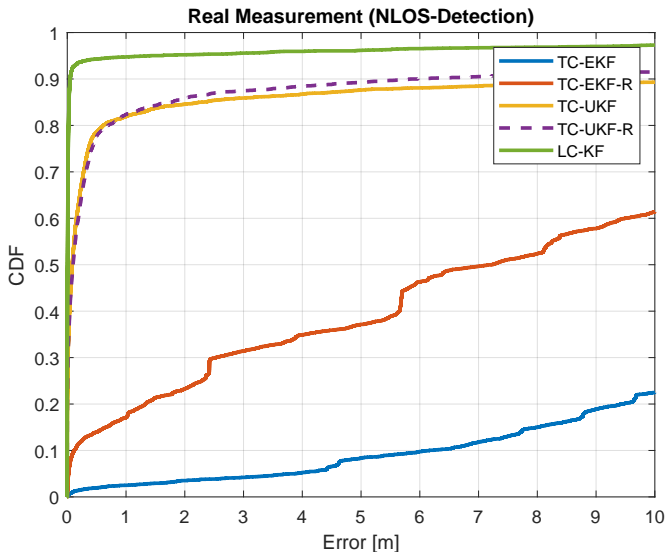


Fig. 16. CDF of the 2D positioning errors while utilizing quasi-real Siradel range and angle measurements with NLoS detection.

tion of both decentralized KF and centralized UKF in three different scenarios. The first scenario, shown in Fig. 17, depicts the performance of the filters when close to a BS while connected to multiple BSs at the same time. It can be seen that the proposed decentralized KF method did not sustain errors while the centralized UKF implementation sustained lane-level errors for short time around the close BS due to linearization errors. The second scenario, shown in Fig. 18, depicts the performance of the filters when they are connected to a single BS. The superiority of the proposed method over centralized UKF can be clearly seen, as the UKF implementation suffered from positioning errors for a longer period of time, due to the lack of supporting BSs. Finally, the third scenario, shown in

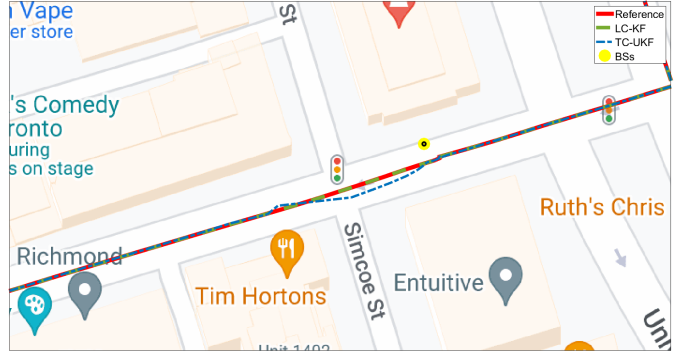


Fig. 17. Close-up performance of filters while driving close to a BS while connected to multiple BSs and using quasi-real measurements.

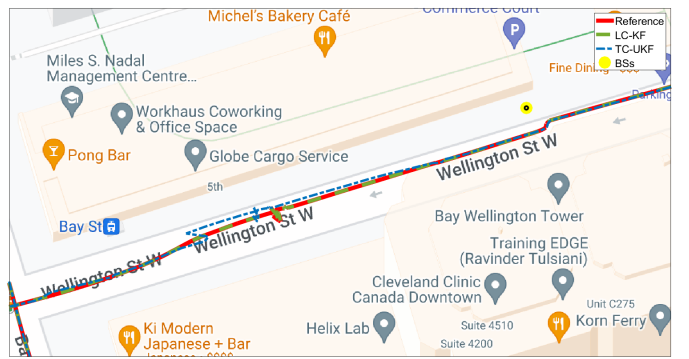


Fig. 18. Close-up performance of filters while driving close to a BS while connected to a single BS and using quasi-real measurements.

Fig. 19, illustrates the performance when the UE is in total NLoS communication with all nearby BSs. It can be seen that both implementations have sustained large amounts of errors. Such a result is expected to occur from time to time while using 5G standalone positioning. Thus, the authors see a crucial need for integration between 5G and other onboard motion sensors to bridge such gaps. Investigation of novel integration methodologies between 5G and other sensors is to be conducted in future works. A summary of the performance statistics of all algorithms and schemes is found in Table I.

TABLE I
2D POSITIONING ERROR STATISTICS SUMMARY

Statistics	LC-KF	TC-UKF	TC-UKF-R	TC-EKF	TC-EKF-R
RMS	12.5m	47.7m	12.8m	881.2m	115.7m
Max	89.9m	885.7m	145.3m	5.8e4m	2.3e3m
< 2m	91.6%	84.5%	85.7%	3.5%	23.3%
< 1m	90.9%	81.9%	82.4%	2.5%	17.1%
< 30cm	90.3%	71.4%	68.9%	1.7%	12.7%

VII. CONCLUSION

In conclusion, it was shown that 5G multi-BS integration schemes for positioning purposes in the literature are heavily

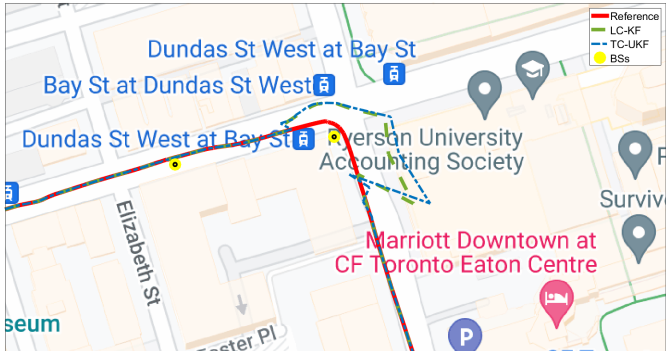


Fig. 19. Close-up performance of filters while driving close to a BS while connected to NLOS BSs and using quasi-real measurements.

inspired by GNSS trilateration centralized schemes. It was proven that such schemes suffer from linearization errors due to the direct use of range and angle measurements. Such errors were necessary for GNSS-based algorithms, as the states and the measurements do not have a one-to-one function, as they rely on range measurements only. In 5G, however, it was shown that with the aid of angle-based measurements, a one-to-one function between the states and the measurements can be achieved, opening the way for integration on the position level rather than on the measurement level. Therefore, it was proposed to adopt a decentralized KF-based integration scheme, which totally eliminates linearization errors. To test the proposed integration scheme, a quasi-real simulation system was utilized to simulate 5G operation in downtown Toronto for a real trajectory that is 1 hour and 15 minutes long. The tests took place in a perfect measurement scenario and in a real measurement scenario with/without NLOS detection capabilities. It was shown that the decentralized positioning scheme was able to outperform its centralized counterpart schemes that utilize EKF-based and UKF-based filters by a considerable margin in all scenarios.

REFERENCES

- [1] T. G. Reid, S. E. Houts, R. Cammarata, G. Mills, S. Agarwal, A. Vora, and G. Pandey, "Localization requirements for autonomous vehicles," *SAE International Journal of Connected and Automated Vehicles*, vol. 2, no. 3, sep 2019. [Online]. Available: <https://doi.org/10.4271%2F12-02-03-0012>
- [2] F. Mogyorósi, P. Revisnyei, A. Pašić, Z. Papp, I. Törös, P. Varga, and A. Pašić, "Positioning in 5G and 6G networks—a survey," *Sensors*, vol. 22, no. 13, 2022.
- [3] P. Nair and A. S. Sarif, "A review on application of global positioning system in construction industry," *Progress in Engineering Application and Technology*, vol. 3, no. 1, p. 249–259, Jun. 2022.
- [4] F. Mazhar, M. G. Khan, and B. Sällberg, "Precise indoor positioning using UWB: A review of methods, algorithms and implementations," *Wireless Personal Communications*, vol. 97, pp. 4467–4491, 2017.
- [5] F. Liu, J. Liu, Y. Yin, W. Wang, D. hai Hu, P. Chen, and Q. Niu, "Survey on WiFi-based indoor positioning techniques," *IET Commun.*, vol. 14, pp. 1372–1383, 2020.
- [6] S. Dwivedi, R. Shreevastav, F. Munier, J. Nygren, I. Siomina, Y. Lyazidi, D. Shrestha, G. Lindmark, P. Ernström, E. Stare, S. M. Razavi, S. Murganathan, G. Masini, Å. Busin, and F. Gunnarsson, "Positioning in 5G networks," *IEEE Communications Magazine*, vol. 59, no. 11, pp. 38–44, 2021.

- [7] R. E. Kálmán, "A new approach to linear filtering and prediction problems," *Journal of Basic Engineering*, vol. 82, no. 1, pp. 35–45, 03 1960.
- [8] H. W. Sorenson and A. R. Stubberud, "Non-linear filtering by approximation of the a posteriori density," *International Journal of Control*, vol. 8, no. 1, p. 33–51, 1968.
- [9] S. Julier and J. Uhlmann, "Unscented filtering and nonlinear estimation," *Proceedings of the IEEE*, vol. 92, no. 3, pp. 401–422, 2004.
- [10] P. Del Moral, "Nonlinear filtering: Interacting particle resolution," *Comptes Rendus de l'Académie des Sciences - Series I - Mathematics*, vol. 325, no. 6, p. 653–658, 1997.
- [11] J. Talvitie, T. Levanen, M. Koivisto, K. Pajukoski, M. Renfors, and M. Valkama, "Positioning of high-speed trains using 5G new radio synchronization signals," in *2018 IEEE Wireless Communications and Networking Conference (WCNC)*, 2018, pp. 1–6.
- [12] J. Talvitie, T. Levanen, M. Koivisto, T. Ihälainen, K. Pajukoski, M. Renfors, and M. Valkama, "Positioning and location-based beamforming for high speed trains in 5G nr networks," in *2018 IEEE Globecom Workshops (GC Wkshps)*, 2018, pp. 1–7.
- [13] J. Talvitie, T. Levanen, M. Koivisto, T. Ihälainen, K. Pajukoski, and M. Valkama, "Positioning and location-aware communications for modern railways with 5G new radio," *IEEE Communications Magazine*, vol. 57, no. 9, pp. 24–30, 2019.
- [14] J. Talvitie, M. Koivisto, T. Levanen, T. Ihälainen, K. Pajukoski, and M. Valkama, "Radio positioning and tracking of high-speed devices in 5G nr networks: System concept and performance," in *2019 27th European Signal Processing Conference (EUSIPCO)*, 2019, pp. 1–5.
- [15] J. Talvitie, T. Levanen, M. Koivisto, and M. Valkama, "Positioning and tracking of high-speed trains with non-linear state model for 5G and beyond systems," in *2019 16th International Symposium on Wireless Communication Systems (ISWCS)*, 2019, pp. 309–314.
- [16] M. Koivisto, M. Costa, A. Hakkarainen, K. Leppanen, and M. Valkama, "Joint 3D positioning and network synchronization in 5G ultra-dense networks using UKF and EKF," in *2016 IEEE Globecom Workshops (GC Wkshps)*, 2016, pp. 1–7.
- [17] G. Americas, "Cellular Communication In a 5G Era," 5G Americas, Tech. Rep., 01 2022.
- [18] Q. Bader, S. Saleh, M. Elhabiby, and A. Noureldin, "NLoS detection for enhanced 5G mmWave-based positioning for vehicular IoT applications," in *Accepted in 2022 IEEE Globecom*, 2022.
- [19] S. Saleh, S. Sorour, and A. Noureldin, "Vehicular positioning using mmWave TDOA with a dynamically tuned covariance matrix," in *2021 IEEE Globecom Workshops (GC Wkshps)*, 2021, pp. 1–6.
- [20] J. Levine, "Fundamentals of 5G small cell deployments," in *2020 IEEE Communications Society Training Course*, 2020.



Sharief Saleh (Graduate Student Member, IEEE) was born in Doha, Qatar, in 1995. He received the B.Sc. and M.Sc. degrees in electrical engineering from Qatar University, Doha, Qatar, in 2016 and 2018 respectively, and is currently pursuing a PhD degree in electrical engineering at Queen's University, Canada. He was awarded a Graduate Assistant position at Qatar University during his master's studies and was then appointed as a Research Assistant at Qatar University, Doha, Qatar. He is currently a member of the Navigation and Instrumentation Research Lab, RMCC. His current research interests include 5G positioning and navigation, sensor fusion, sensors and instrumentation, signal processing, reinforcement learning, and AI.



Qamar Bader (Graduate Student Member, IEEE) received her B.Sc. degree in electrical engineering from Qatar University, Doha, Qatar, in 2016 and is currently pursuing an MSc degree in electrical engineering at Queen's University, Canada. She is currently a member of the Navigation and Instrumentation Research Lab, RMCC. Her current research interests include 5G positioning and navigation, sensor fusion, deep learning, computer vision, and environment mapping.



Mohamed Elhabiby was the Treasurer of the Geodesy Section at the Canadian Geophysical Union from 2008 to 2014. He is currently an Associate Professor with the Faculty of Engineering, Ain Shams University, Cairo, Egypt. He is also the Executive Vice President and a Co-Founder of Micro Engineering Tech Inc., Calgary, AB, a high-tech international company, specialized in high precision engineering and instrumentation, mobile mapping, laser scanning, deformation monitoring, and GPS/INS integrations. He is a Leader of an Archaeological Mission in the Area of Great Pyramids, Cairo. He received the Astech Awards. He is named by Avenue Magazine as one of the Top 40 under 40. He is the Chair of WG 4.1.4: Imaging Techniques, Sub-Commission 4.1: Alternatives and Backups to GNSS. He chaired the Geocomputations and Cyber Infrastructure Oral Session at the Canadian Geophysical Union annual meeting from 2008 to 2012.



Aboelmagd Noureldin (Senior Member, IEEE) received the B.Sc. degree in electrical engineering and the M.Sc. degree in engineering physics from Cairo University, Egypt, in 1993 and 1997, respectively, and the Ph.D. degree in electrical and computer engineering from the University of Calgary, AB, Canada, in 2002. He is currently a Professor with the Department of Electrical and Computer Engineering, Royal Military College of Canada (RMCC) with Cross Appointment at the School of Computing and the Department of Electrical and Computer Engineering, Queen's University. He is also the Founder and the Director of the Navigation and Instrumentation Research Lab, RMCC. He has published two books, four book chapters, and more than 270 papers in journals, magazines, and conference proceedings. His research interests include global navigation satellite systems, wireless location, and navigation, indoor positioning, and multi-sensor fusion targeting applications related to autonomous systems, intelligent transportation, road information services, crowd management, and the vehicular Internet of Things. His research work led to 13 patents and several technologies licensed to the industry in the area of position, location, and navigation systems.